Formation and growth of ultrafine particles from secondary sources in Bakersfield, California

Lars Ahlm,[1] Shang Liu,[1] Douglas A. Day,[1,2] Lynn M. Russell,[1] Robin Weber,[3] Drew R. Gentner,[4] Allen H. Goldstein,[3,4] Josh P. DiGangi,[5] Samuel B. Henry,[5] Frank N. Keutsch,[5] Trevor C. VandenBoer,[6] Milos Z. Markovic,[6] Jennifer G. Murphy,[6] Xinrong Ren,[7,8] and Scott Scheller[9]

Received 9 November 2011; revised 12 January 2012; accepted 16 January 2012; published 7 March 2012.

[1] In this study, physical and chemical properties of ultrafine aerosol particles are investigated at an urban site in Bakersfield, California, during the CalNex 2010 (California Research at the Nexus of Air Quality and Climate Change) campaign in May and June. Ultrafine particle measurements include particle number size distributions by a scanning Differential Mobility Analyzer (DMA) and size resolved aerosol chemical composition determined with a High-Resolution Time-of-Flight Aerosol Mass Spectrometer (HR-ToF-AMS). Growth events of ultrafine particles were observed on most days and had a very regular pattern. A nucleation mode centered at ~20 nm appeared in the morning and grew to 40–100 nm throughout the day. Microphysical modeling and size-resolved HR-ToF-AMS concentrations showed that organic components provided most of the particle growth in the ultrafine mode, and sulfate provided on most days only a minor contribution to the mass of this mode. The ultrafine particle mass was largely dominated by organics (77%), and was at maximum during the afternoon. Elemental carbon (EC) and the AMS tracer $C_4H_9^+$ for hydrocarbon-like organic aerosol (HOA) peaked in the early morning during rush hour, indicative of primary emissions. The fact that the particle number concentration peaked in the afternoon, when EC was at minimum, indicates that the midday increase in number concentration was likely due to new particle formation. The potential importance of solar radiation, the condensation sink of vapor on existing particles, concentrations of OH, O_3, SO_2, NH_3, and VOCs for both condensational growth and new particle formation is evaluated based on the covariation of these parameters with ultrafine mass. The results suggest that the ultrafine particles are from secondary sources that are co-emitted or co-produced with glyoxal and formaldehyde.

Citation: Ahlm, L., et al. (2012), Formation and growth of ultrafine particles from secondary sources in Bakersfield, California, *J. Geophys. Res.*, *117*, D00V08, doi:10.1029/2011JD017144.

1. Introduction

[2] There is extensive evidence that aerosol particle pollution has adverse effects on human health [e.g., *Pope and Dockery*, 2006; *Harrison et al.*, 2010]. Aerosols in many locations are regulated by particle mass, for instance $PM_{2.5}$ (mass concentration of particles with diameter D_p lower than 2.5 μm). However, urban particle number size distributions are in general observed to have their peak number concentration at a diameter of 20–40 nm [*Shi et al.*, 1999; *Woo et al.*, 2001; *Ketzel et al.*, 2004; *Stanier et al.*, 2004a]. Particles in this size range often make a relatively low contribution to the $PM_{2.5}$ aerosol mass. Nevertheless, results from several studies indicate that ultrafine particles (D_p < 100 nm) may cause particularly adverse health effects [e.g., *Oberdörster et al.*, 1995; *Peters et al.*, 1997]. Aerosol particles also influence the Earth's climate, and the radiative forcing from anthropogenic particles being activated as cloud condensation nuclei (CCN) in clouds represents one of

[1]Scripps Institution of Oceanography, University of California, San Diego, La Jolla, California, USA.
[2]Now at Cooperative Institute for Research in the Environmental Sciences, University of Colorado at Boulder, Boulder, Colorado, USA.
[3]Department of Environmental Science, Policy, and Management, University of California, Berkeley, California, USA.
[4]Department of Civil and Environmental Engineering, University of California, Berkeley, California, USA.
[5]Department of Chemistry, University of Wisconsin-Madison, Madison, Wisconsin, USA.
[6]Department of Chemistry, University of Toronto, Toronto, Ontario, Canada.
[7]Rosenstiel School of Marine and Atmospheric Science, University of Miami, Miami, Florida, USA.
[8]Now at Air Resources Laboratory, National Oceanic and Atmospheric Administration, Silver Spring, Maryland, USA.
[9]California Air Resources Board, Sacramento, California, USA.

0148-0227/12/2011JD017144

the largest uncertainties in the climate system [e.g., *Rosenfeld*, 2006].

[3] In urban areas, motor vehicles are a major aerosol source, in particular in the ultrafine size range. Vehicle exhaust can be broadly divided into a nanoparticle mode (D_p < 30 nm), which dominates the exhaust particle number, and an accumulation mode (30 nm < D_p < 500 nm). While nanoparticles from vehicle emissions are composed primarily of semi-volatile organics and sulfur compounds, and are formed by nucleation in the tailpipe or ~0.1 s after exiting the tailpipe, the accumulation mode is composed primarily of soot cores coated with sulfate and organic species [*Kittelson et al.*, 2006].

[4] Apart from emissions at the surface, particles may also form in the atmosphere during events of new particle formation [e.g., *Kulmala et al.*, 2004]. In general, new particle formation is favored by low concentrations of pre-existing aerosol particles because there is competition between vapor condensation on preexisting particles and new particle formation. Despite this, new particle formation events and subsequent growth have been regularly observed at several polluted urban sites including Leipzig [*Birmili and Wiedensohler*, 2000], Atlanta [*Woo et al.*, 2001], Pittsburgh [*Stanier et al.*, 2004b], Birmingham, UK [*Alam et al.*, 2003], Mexico City [*Dunn et al.*, 2004] and Beijing [*Wu et al.*, 2007]. Newly formed particles can grow in the atmosphere by condensation of low volatility vapors.

[5] In almost all studies, sulfuric acid concentrations were observed to be too low to explain the observed particle growth rates [e.g., *Alam et al.*, 2003, *Smith et al.*, 2008; *Riipinen et al.*, 2011]. In those studies, the largest contribution to condensational growth came from condensation of organic compounds. Volatile organic compounds (VOCs) can have anthropogenic or biogenic sources and are oxidized in the atmosphere primarily by OH, O_3 and NO_3. This atmospheric oxidation can lead to a high number of different oxidation products that may have lower volatility than their parent VOCs. Organic vapors with low enough volatility can partition into the particle phase and thereby contribute to condensational growth. However, partly because the number of oxidation products is extremely high, large uncertainties remain in regards to what specific compounds contribute to condensational growth [*Hallquist et al.*, 2009].

[6] In this study we present results from size-resolved measurements of ultrafine aerosol particles at a polluted urban site in Bakersfield, California, where growth events of ultrafine particles were observed on 39 of 45 days. The source of the seed particles, the chemical properties of the ultrafine aerosol, and parameters relevant for the growth are investigated. This study was carried out as part of the CalNex (California Research at the Nexus of Air Quality and Climate Change) campaign at the Bakersfield Supersite in May and June 2010.

2. Site and Methods

2.1. Field Site and Meteorology

[7] The measurements in this study were performed at the CalNex supersite in Bakersfield, California (35.35°N, 118.97°W). The site is located about 4 km to the southeast of the city center (Figure 1). The freeway State Route (SR) 58 passes about 800 m to the north, and the SR 99 passes 7 km to the west. The highway SR 184 is located about 4 km to the east of the site. The average wind direction included in the map over Bakersfield in Figure 1 indicates that the air most of the time was not advected from the city center to the sampling site.

[8] Bakersfield was chosen as the site for this project because of its high PM concentrations. The city is located in the southern end of the Central Valley, which stretches 720 km from the Cascade Mountains in the northwest to the Tehachapi Mountains in the southeast. The Central Valley is bordered to the west by the Coastal Ranges and to the east by the Sierra Nevada Mountains. The San Joaquin Valley comprises the southern part of Central Valley and is one of the largest $PM_{2.5}$ and PM_{10} non-attainment areas in the United States. The geographical boundaries with the surrounding mountains and the meteorology play important roles in accumulating pollutants in the valley, in particular during times of day when the atmospheric boundary layer is shallow and ventilation is limited [*Chow et al.*, 2006].

[9] Previous studies have shown that the prevailing summertime wind pattern is dominated by marine air that penetrates through the Carquinez Strait and splits into two currents when entering the Central Valley, one flowing northeastward toward Sacramento and one flowing southeastward toward San Joaquin Valley [*Moore et al.*, 1987; *Zaremba and Carroll*, 1999; *Zhong et al.*, 2004]. Figure 1 shows an analysis of back trajectories during the measurements in this study obtained using NOAA's Hybrid Single Particle Lagrangian Integrated Trajectory (HYSPLIT) model with meteorological data sets from Eta Data Assimilation System (EDAS40). The color indicates the number of trajectories that have passed through a certain grid cell. There is a very strong preponderance of trajectories entering Bakersfield from the northwest, consistent with the discussion above, even though most of the trajectories enter the continent at Monterey Bay, south of San Francisco and south of the Carquinez Strait. There are also a relatively large number of trajectories entering Bakersfield from a westerly direction without any northerly component. However, the influence of pollution from Los Angeles in the south should be negligible.

[10] The local wind directions were predominantly northwesterly in daytime. However, during some nights the wind direction shifted to the east or south, associated with downslope flows from the surrounding mountains as discussed by *Zhong et al.* [2004]. The median maximum diurnal wind speed was ~4 m s^{-1} peaking around 17:00 and the corresponding median minimum value was 1.5 m s^{-1}, occurring around 06:00. The median maximum diurnal temperature during this campaign was 29.5°C peaking around 16:00, the same time as the relative humidity reached its minimum value of ~22%. The median of the diurnal minimum temperature was 16°C, occurring at 05:00, coinciding with a peaking relative humidity of ~60%. The campaign was dominated by cloud free conditions or very low cloudiness, except during a few days in the beginning of the campaign when some rainfall occurred. Apart from the nights on May 18 and May 19, when the relative humidity peaked at 96% and 88%, respectively, the relative humidity never exceeded 82%, indicating mostly dry conditions during the campaign.

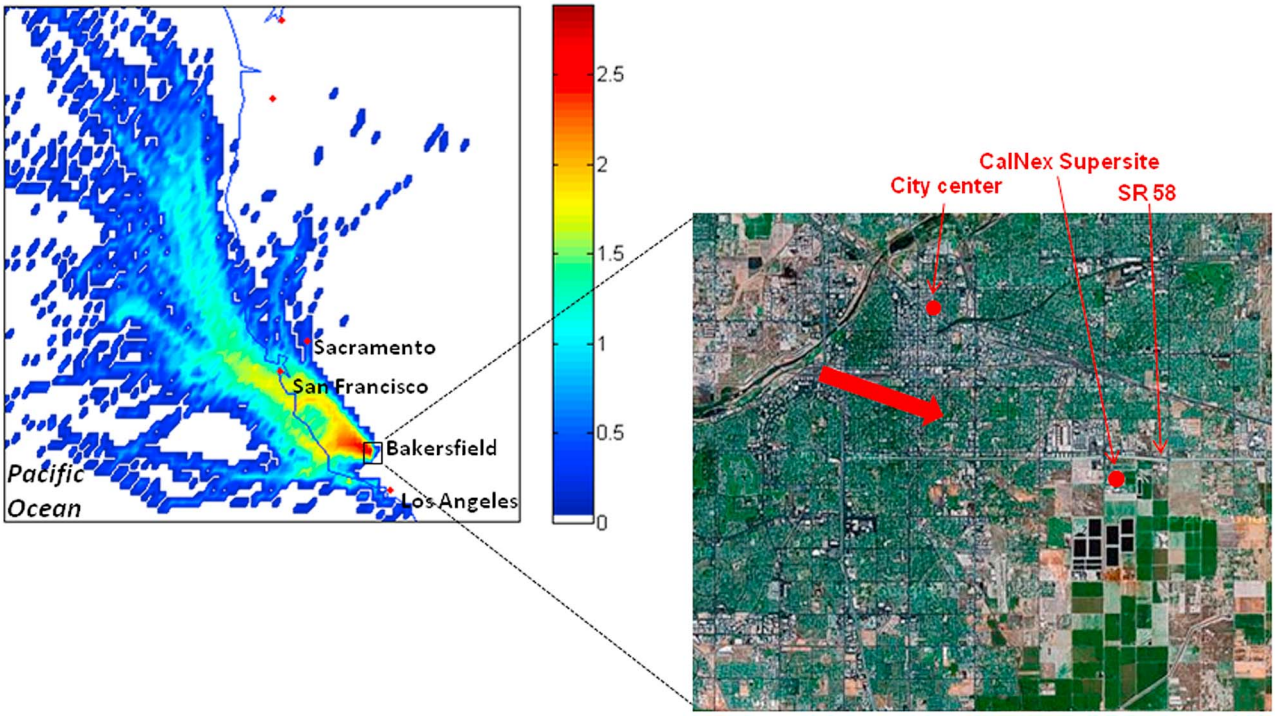

Figure 1. (left) HYSPLIT back trajectory (72 h) analysis for trajectories initiated at Bakersfield. The color scale indicates $\log_{10}$ of the number of trajectories that have passed (through a certain grid cell. The grid cells are 0.2 degrees wide in both latitudinal and longitudinal direction. For every day 12 back trajectories have been calculated with an interval of two hours between each trajectory. (right) Map (from Google) showing the location of the CalNex Supersite in Bakersfield. The red arrow indicates the most frequent wind direction at the site.

[11] *Zhong et al.* [2004] investigated the atmospheric boundary layer in the Central Valley during summertime and found that the afternoon mixed layer was in general deeper than 1000 m, and that the mixed layer depth increased with distance away from the ocean and southwards in the Central Valley. At night, they observed a temperature inversion develop in the lowest few hundred meters.

[12] In this study we have used the HYSPLIT model to get rough estimates of diurnal variations in boundary layer depth during the campaign in Bakersfield. The model indicates that the mixed layer started growing soon after sunrise around 06:00 and often reached its full depth of ~2 km around 17:00. According to the model, the nocturnal boundary layer was about 100 m deep. Although the depth of the nocturnal inversion from the HYSPLIT model is likely to be associated with large uncertainties, there is a very sharp contrast in boundary layer depth between day and night. The shallowness of the nocturnal boundary layer enhances the impact from surface emissions on local concentrations, which may allow pollutant concentrations to build up at night and in the early morning during rush hour.

2.2. Experimental Setup

[13] Particle number size distributions were measured using a scanning Differential Mobility Analyzer (DMA). The DMA is a TSI column with a TSI 3010 CPC running Labview-based software from *Collins et al.* [2004], modified for negative charging efficiency. Size-resolved number concentrations in 60 size bins from a particle diameter of 10 nm up to 1 μm were collected, and duplicate (upward and downward) mobility scans were completed every 11 min.

[14] Aerosol chemical composition, including all species that are vaporized at a temperature of 600°C, was measured using an Aerodyne High-Resolution Time-of-Flight Aerosol Mass Spectrometer (HR-ToF-AMS). This instrument provides size-resolved mass concentrations in an approximate vacuum aerodynamic particle diameter range of 0.03 to 1.0 μm. Prior to the start of the campaign, the flow rate of the HR-ToF-AMS was calibrated, and the lens of the AMS was aligned to a position where ~100% of the 350 nm particles reach the vaporizer of the AMS. Under this configuration particles from ~50–600 nm are expected to be transmitted with ~100% efficiency. A size/velocity calibration, which relates particle time of flight (ToF) velocity to aerodynamic particle size, was also performed before the campaign started. The ionization efficiency (IE) calibration was performed about twice a week during the campaign. During this calibration, dry ammonium nitrate particles generated by an atomizer with D_p = 300–350 nm were used to ensure close to 100% transmission efficiency. The collection efficiency (CE) of the AMS was estimated to be 0.8 based on scaling the AMS mass to the scanning DMA mass (minus the elemental carbon (EC) mass and estimated dust). The vacuum aerodynamic diameter of the AMS has been recalculated to mobility diameter to make it possible to compare with the scanning DMA data in this study. The relation between mobility diameter (D_m) measured by the scanning DMA and vacuum aerodynamic diameter (D_{va})

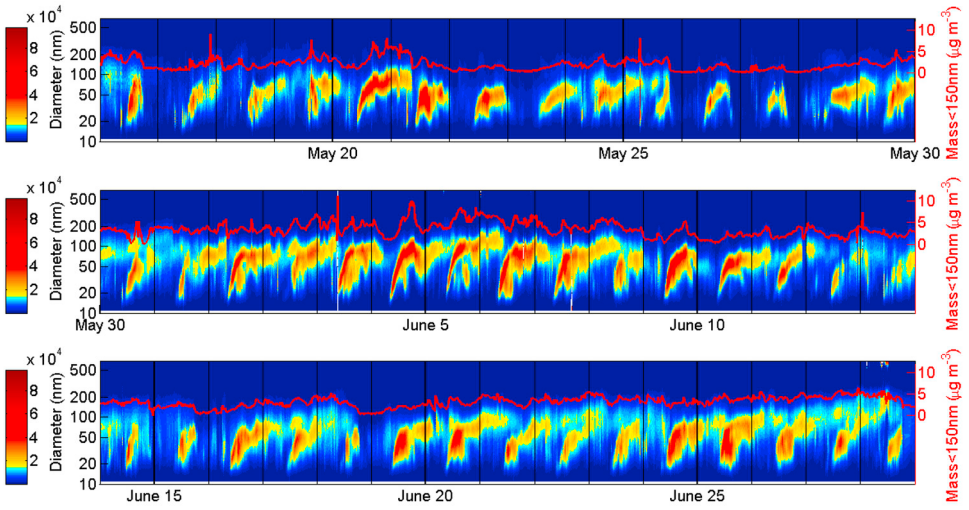

Figure 2. Time series of the particle number size distribution for the whole campaign. The color scale represents $dN/dlogD_p$ (cm^{-3}) and the vertical black grid lines indicate midnight. The red curve represents mass of particles with a diameter lower than 150 nm derived from the SMPS size distributions with an assumed particle density of 1.4 g cm^{-3} (section 2.2).

measured by the AMS is for spherical particles [e.g., *Kostenidou et al.*, 2007]:

$$D_m = \frac{D_{va}}{\rho}\rho_0 \quad (1)$$

where ρ is the effective density and ρ_0 is unity. In this study we found the best agreement in average mass distributions from the scanning DMA and AMS for an average ρ of 1.4 g cm^{-3}.

[15] Gas-phase measurements of SO_2, ammonia, formic acid and oxalic acid were made by Ambient Ion Monitor Ion Chromatograph (AIM-IC). The instrument consists of an AIM 9000D air sampler (URG Corp., Chapel Hill, NC), a constantly generated wet parallel-plate denuder with 5 mM H_2O_2 eluent for the collection of gases, and two ICS-2000 ion chromatographs (Dionex Corp., Sunnyvale, CA). The sample collection components of the instrument were located in a separate housing unit, which was specifically built for this study. In this novel instrument configuration gases were stripped into solution in a tower-mounted assembly to minimize sampling inlet losses for soluble gases such as NH_3 and HNO_3.

[16] UV radiation was measured by a semiconductor photodiode with a spectral response range from 280 to 360 nm. The sensor was calibrated again a Yankee Environmental Systems' Ultraviolet Pyranometer (Model UVB-1) in natural sunlight.

[17] OH concentration was determined using a Ground-based Tropospheric Hydrogen Oxides Sensor (GTHOS) based on laser induced fluorescence, and ozone was measured with a Dasibi 1008 PC monitor. The gas-phase concentration of formaldehyde was determined using Fiber Laser-Induced Fluorescence [*DiGangi et al.*, 2011] and the gas-phase glyoxal concentration was obtained with Laser-Induced Phosphorescence [*Huisman et al.*, 2008]. A broad suite of primary and secondary VOCs were measured with hourly time resolution using a gas chromatograph equipped with both a mass spectrometer and a flame ionization detector.

[18] EC was measured with a thermal-optical carbon aerosol analyzer from Sunset Laboratory (Oregon, USA) using a modified IMPROVE-A protocol, operated by the California Air Resource Board.

3. Results and Discussion

[19] The measurements in this study were performed between 15 May and 29 June, 2010. The average number concentration in the total scanning DMA size range (D_p = 0.01–1 μm) was 10300 cm^{-3}. The average number concentration of ultrafine particles (D_p < 100 nm) was 8600 cm^{-3}. Hence, the aerosol number population was strongly dominated by ultrafine particles during this campaign.

3.1. Ultrafine Particle Growth Events

[20] Figure 2 illustrates how the size-resolved number concentration varied throughout the measurement period. In this figure it can be seen that growth of small 15–20 nm particles up to 40–100 nm occurred on almost all days. What is striking is the regularity and the large number of particle growth events for an urban site. Specifically, ultrafine particle growth for at least three hours and at least up to 40 nm could be clearly observed on 39 out of 45 days. It can also be seen in Figure 2 that the growth events on many days have a large impact on the aerosol mass, which means that it is possible to investigate the chemical composition of the growing particles. Mass size distributions from the AMS during ultrafine growth events are presented in section 3.2.

[21] Since the growth events varied in mass change, size change, and duration, it is not meaningful to present an average particle number size distribution for the whole campaign. Rather, it is more interesting to investigate the evolution of the size distributions during different time periods of typical days. Figure 3a shows the average particle number size distribution in different two hour intervals

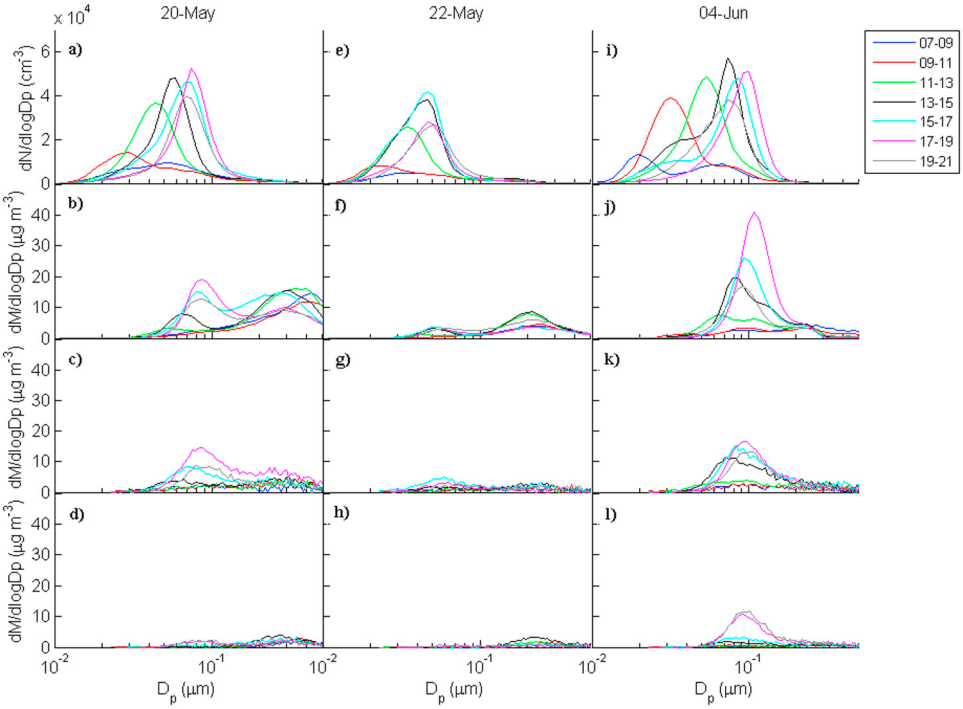

Figure 3. Temporal evolution of aerosol size distributions between 07:00 and 21:00, averaged over two-hour intervals, on three different days. (a, e and i) Scanning DMA particle number size distributions on 20 May (Figure 3a), 22 May (Figure 3e) and 4 June (Figure 3i). (b, f and j) Calculated mass size distributions (using the number size distributions) for the same days with an assumed particle density of 1.4 g cm^{-3}. (c, g and k) AMS organic mass size distributions and (d, h and l) AMS sulfate mass size distributions for the same days.

throughout the 24 h of 20 May 2010. This figure illustrates the regular pattern of these growth events. On average, a mode of nanoparticles centered at ~15–20 nm appeared around 09:00 in the morning. In addition to this nanoparticle mode, a pre-existing Aitken mode centered at ~60 nm can be seen. Throughout the morning and most of the afternoon, the number concentration of the nanoparticle mode increases considerably. Meanwhile, the mode shifts to larger diameters when the particles grow, producing an increasingly unimodal size distribution below ~150 nm. Between 13:00 and 15:00, the mode is on average centered at 60 nm. Throughout the evening and night, the growth did often continue, but the number concentration decreased. Since these growth events could be observed clearly for several hours on most days during the campaign, the events must be fairly regionally homogeneous with limited horizontal variability in vapor and particle concentrations. Growth events could be followed from morning until at least 18:00 in the evening for 31 of the 39 observed growth events. For some of the other eight events, growth may have continued until 18:00 but could not be followed all the way because the growing nanoparticle mode and the preexisting Aitken mode could not be separated. A growth event that lasts for about ten hours under an assumed wind speed of 3 m s^{-1} gives a horizontal scale of more than 100 km, making these events important regionally for ultrafine particle concentrations.

[22] An interesting question is, from where do the ~15–20 nm particles that appear in the morning (and afternoon) originate? Are they associated with emissions of small particles or do they originate from new particle formation? As mentioned in the introduction, vehicles emit nanoparticles in this size range. However, the fact that the nanoparticle mode was often centered around 15–20 nm when it appeared does not necessarily imply that the particles originate from primary emissions. Brownian diffusion is efficient for 10–20 nm particles, which means that concentrations of the smallest particles are underestimated due to losses in the sampling line. However, the loss by Brownian diffusion in the sampling line was estimated to be less than 10% for 10 nm particles, which is too low to explain the lower concentrations of 10 nm particles relative to the concentrations of ~20 nm particles. Another possibility is that new particle formation occurs before reaching the Bakersfield sampling site but is suppressed in the city where background aerosol concentrations are higher, or that the formation occurs in the residual layer above the growing mixed layer. Then the particles would have some time to grow before being measured by the scanning DMA. Due to the fact that no particle measurements below 10 nm were performed in this field study, there is no direct proof of whether new particle formation or vehicle emission is the mechanism responsible for the production of the observed nanoparticles. However, comparing the diurnal cycle of particle number concentration with that of tracers, it is possible to indirectly show that new particle formation is likely the most important source for these nanoparticles. This investigation will be presented and discussed in section 3.3.

[23] The growth during the events was in general linear with time until around 13:00, but often decreased in rate throughout the afternoon and evening. Growth rates have been determined by calculating linear fits of the growth of the center of the mode while the growth was linear. The rates varied between 2.9 and 14.9 nm hr^{-1} during the campaign. The average growth rate was 7.3 nm hr^{-1} with a standard deviation of 2.6 nm hr^{-1}. This is within the range of what has been observed at several other urban sites, for instance Atlanta [*Stolzenburg et al.*, 2005], Mexico City [*Dunn et al.*, 2004], Leipzig [*Birmili and Wiedensohler*, 2000], Budapest [*Salma et al.*, 2011] and Beijing [*Wu et al.*, 2007].

3.2. Classification of Growth Events and Chemical Composition of Growing Particles

[24] The growth events were divided into three classes: High growth (HG) days, low growth (LG) days and non-event (NE) days. HG days were defined as days when the growing mode reached 70 nm before 18:00. LG days were defined as days with growth for at least three hours and up to 40 nm (but less than 70 nm) before 18:00. Remaining days were defined as non-event (NE) days. Eleven days fell into the HG class, 28 days fell into the LG class, and 6 days were NE days. Figure 3 shows two examples of HG days (20 May and 4 June) and one example of an LG day (22 May) with two-hour averages of scanning DMA and AMS size distributions.

[25] On 20 May a nucleation mode appears in the number size distribution representing 09:00–11:00 (Figure 3a), and is followed by growth throughout the day. By 13:00–15:00 the center of the mode has grown to a diameter of 60 nm and at this point the mode starts to make a clear impact also in the mass size distribution (Figure 3b). The AMS organic (Figure 3c) and sulfate (Figure 3d) mass size distributions show that almost all mass in this growing size range consists of organic components. The growth continues until 17:00–19:00 and the center of the mode reaches a final diameter of 80 nm. The mass is still dominated by organics.

[26] Also on 22 May, a nucleation mode appears at 09:00–11:00 followed by growth (Figure 3e). However, the growth slows down after 13:00–15:00 and the mode does not reach further than 50 nm. Due to the limited growth on 22 May, the aerosol mass increase caused by the growth is considerably lower than the corresponding mass increase on 20 May (Figure 3f). However, also on 22 May almost all the growth seems to have been associated with condensation of organic vapors (Figure 3g), and the contribution from sulfate is low (Figure 3h).

[27] On 4 June, a nucleation mode appears already at 07:00–09:00 (Figure 3i). The growth continues until 17:00–19:00 and the center of the mode reaches a diameter of nearly 100 nm with a large increase in mass as result (Figure 3j). From the organic and sulfate mass size distributions (Figures 3k and 3l), it is clear that organics are responsible for almost all growth until 15:00–17:00. At this point the mode has reached a diameter of 80 nm. However, during the next growth phase from 80 to 100 nm sulfate actually makes the largest contribution. The growth event on 4 June was the event with the largest contribution from sulfate of all events during the campaign.

[28] Some of the most distinct growth events with two-hour averaged chemical composition of the aerosol mass below 150 nm can be seen in Figure 4. The growth events affected the mass size distributions well above 100 nm on days with the highest growths. Therefore the size distributions have been cut at 150 nm here to include most of the mass increase during the growth events. The growth events in Figure 4 are on most days accompanied by an increase in aerosol mass. The exception to this trend is the relatively high aerosol mass at 06:00–08:00 on some days associated with aerosol mass of the preexisting mode. Organics strongly dominate the addition of mass during most of the growth events in Figure 4. Particularly from morning until 12:00–14:00 the growth and mass are nearly exclusively associated with organic components. However, especially on 4 June the contribution from sulfate somewhat increases during late afternoon or early evening (as seen also in Figure 3l). There was also a tendency of slightly increasing ammonium when sulfate increased, indicating that most of the sulfate was in the form of ammonium sulfate and ammonium bisulfate.

3.3. Diurnal Cycles of Tracers for Primary and Secondary Aerosols

[29] The composition of the growing particles during the frequent ultrafine growth events in Figure 2 indicate that most of the total ultrafine particle mass is organic, and the midday timing of these events (as well as the lack of an afternoon peak in EC) indicates that they are secondary (formed in the atmosphere). This section will focus on the chemical compounds that dominate the ultrafine particle mass, the contribution from primary emissions and secondary aerosol formation to the ultrafine particle mass, and the production mechanism responsible for the frequently observed 15–20 nm particles that provide seeds for the subsequent growth.

[30] The growth events observed in this study are highly regular. They occur almost every day and start in the morning (Figures 2 and 3). During this campaign, organic components represented 77% of the ultrafine aerosol mass (D_p < 100 nm), thereby strongly dominating the ultrafine mass. Sulfate represented the second largest non-refractory mass contribution with 16%. Ammonium provided a minor contribution (5%) and nitrate was only 2%. In Pittsburgh [*Zhang et al.*, 2004], nitrate was also observed to be a minor component in the ultrafine size range. However, the organic fraction in the ultrafine range is much higher in Bakersfield than what was observed in Pittsburgh where the summertime fraction was 45% [*Stanier et al.*, 2004a]. Accordingly, the sulfate fraction is significantly lower in Bakersfield than what was observed in Pittsburgh, where 40% of the ultrafine mass was salts of ammonium and sulfate.

[31] The AMS mass spectral peak at the mass-to-charge ratio (m/z) 57 is often used as a tracer for hydrocarbon-like organic aerosols (HOA), whereas m/z 44 works as a tracer for oxygenated organic aerosols (OOA) [*Zhang et al.*, 2005; *Russell et al.*, 2009]. The m/z 57 include the ion peaks of $C_4H_9^+$ and $C_3H_5O^+$, and m/z 44 include the ion peaks of CO_2^+ and $C_2H_4O^+$. Here we present the non-oxygenated fragment $C_4H_9^+$ as a tracer for HOA and the oxygenated fragment CO_2^+ as a tracer for OOA.

[32] Figure 5 shows median diurnal cycles of EC, $C_4H_9^+$, CO_2^+, organic mass, total particle number concentration and vapor condensation sink (*CS*) for HG (Figures 5a–5c) and

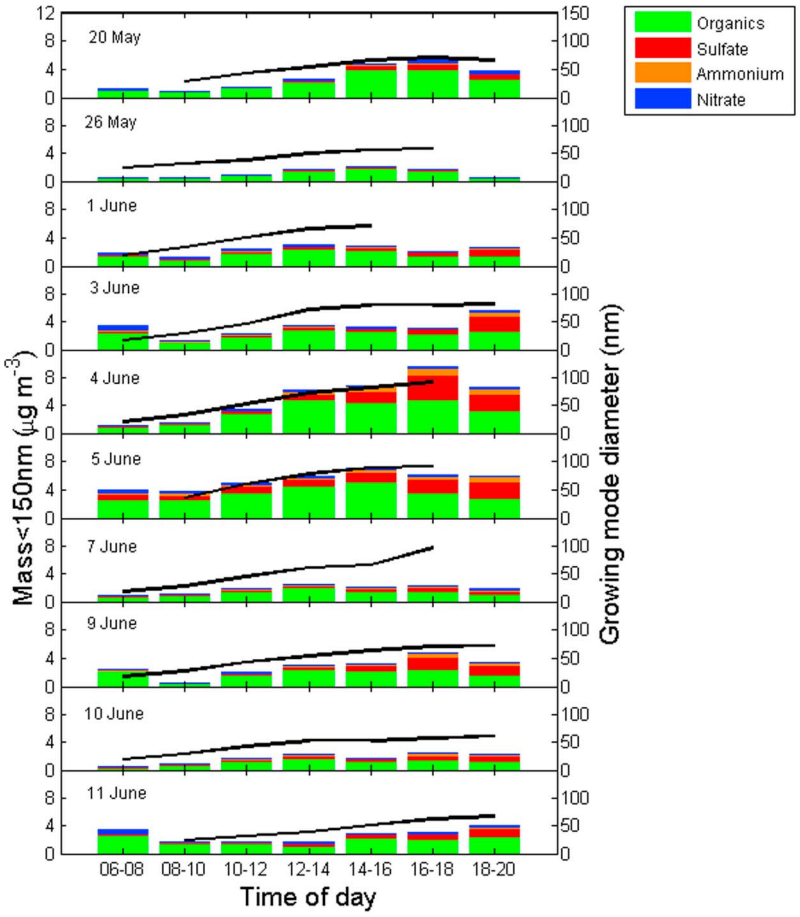

Figure 4. Aerosol chemical composition of the growing mode during ten different days. The AMS mass size distributions have been cut at 150 nm. The black curves represent the diameter associated with the center of the growing mode.

LG (Figures 5d–5f) days. Only particles with diameters lower than 150 nm have been included in the diurnal cycles of $C_4H_9^+$, CO_2^+ and organic mass. The reason for selecting 150 nm as the cutoff for ultrafine particles was to include most of the mass increase associated with the growth events, as discussed in section 3.2. The *CS* determines the rate of condensation of molecules onto pre-existing particles [e.g., *Kulmala et al.*, 2001]; it is defined as:

$$CS = 2\pi D \sum_{i}^{n} \beta(D_{p,i}) D_{p,i} N_i \qquad (2)$$

where D is the diffusion coefficient of the condensing vapor (here as assumed to be 0.1 $cm^2\ s^{-1}$), $D_{p,i}$ is the particle diameter of bin i, β is the transition regime correction factor [*Fuchs and Sutugin*, 1971], N_i is the number concentration within size bin i, and n is the number of size bins. We have assumed the accommodation coefficient to be unity.

[33] In general, the diurnal cycles of EC and $C_4H_9^+$ are rather similar both on HG (Figure 5a) and LG (Figure 5d) days. Concentrations are high at nighttime and peak early in the morning around 07:00 during rush hour. A peak in aerosol number concentrations due to primary emissions early in the morning have been observed in several other urban studies [e.g., *Woo et al.*, 2001; *Harrison and Jones*, 2005; *Kalafut-Pettibone et al.*, 2011]. High traffic in the morning results in high aerosol emissions. Furthermore, the fact that the boundary layer is shallow at this point means that particle emissions will have a large impact on the observed concentration. After ~08:00 both EC and $C_4H_9^+$ start decreasing to reach a minimum later in the day. This is likely to a large extent caused by dilution through entrainment when the mixed layer grows. Around 16:00, $C_4H_9^+$ experiences a second smaller peak concentration, while EC stays low. The rush hour peaks in the morning are somewhat larger in the HG diurnal cycles than in the LG cycles. Higher primary emissions of EC and organic particles on HG days are likely accompanied by higher primary emissions of anthropogenic VOCs that may contribute to more efficient condensational growth on these days.

[34] The median diurnal cycles of CO_2^+ (Figures 5b and 5e), the tracer for OOA, shows a different pattern and shows a second and larger peak concentration in afternoon, which indicates that photochemistry plays an important role in the production of SOA. The relative increase in $C_4H_9^+$ during afternoon is much lower than the corresponding increase in CO_2^+, and the ratio between CO_2^+ and $C_4H_9^+$ is on HG days at maximum around 16:00. Interestingly, the diurnal cycles of

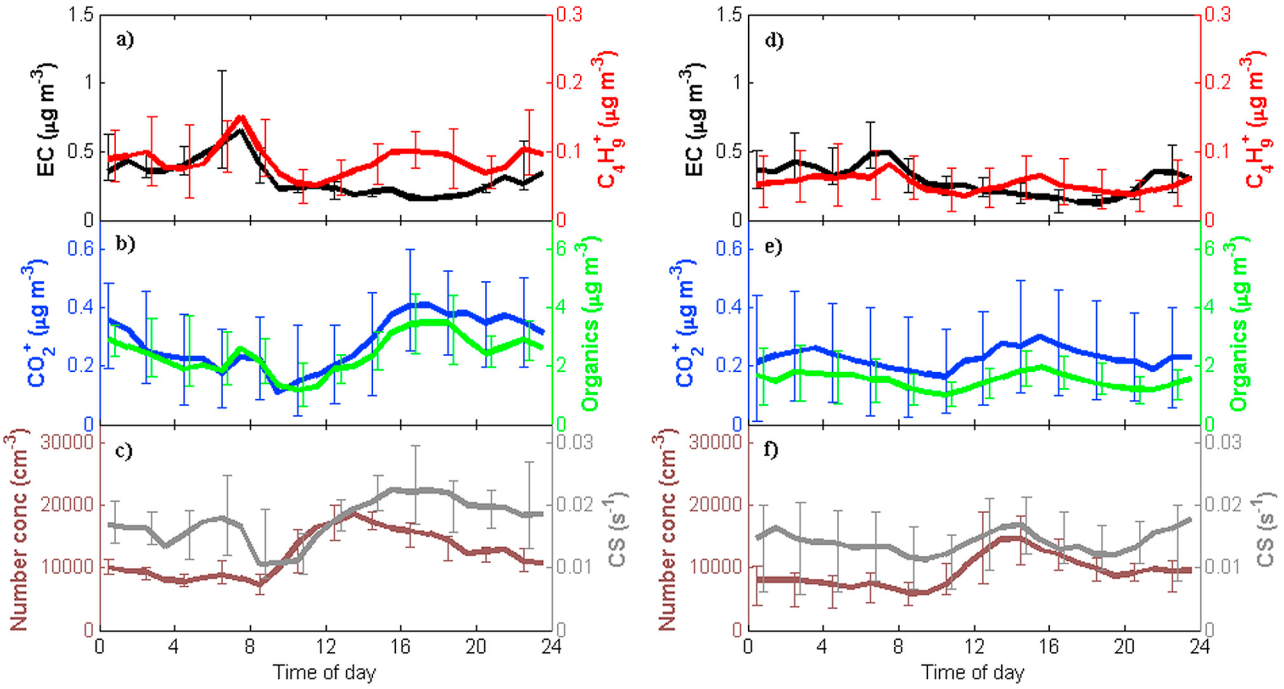

Figure 5. Median diurnal cycles of EC (black), $C_4H_9^+$ (red), CO_2^+ (blue), organic mass (green), particle number concentration (brown) and condensation sink (gray). (a, b and c) Only high growth (HG) days have been included. (d, e and f) Only low growth (LG) days have been included. In the diurnal cycles of $C_4H_9^+$, CO_2^+ and organic mass, only particles with a diameter lower than 150 nm have been included.

organic mass (Figures 5b and 5e) look very similar to the CO_2^+ diurnal cycles, and have their maximum values during the afternoon at the same time as CO_2^+. The afternoon maxima in CO_2^+ and organic mass concentration are higher on HG days than on LG days, consistent with more SOA formation on HG days. The early morning peak observed in EC and $C_4H_9^+$ on LG days (Figure 5d) is not present in the diurnal cycle of organic mass (Figure 5e), indicating that the mass contribution from primary emissions to the organic mass below 150 nm is low on LG days. Also on HG days, the morning peak in organic mass (Figure 5b) is small compared to the afternoon peak, indicating that primary emissions make a low relative contribution to the organic mass below 150 nm also on HG days. Instead the organic mass is dominated by photochemically produced SOA.

[35] The median diurnal cycles of total (0.01–1.0 μm) particle number concentration (Figures 5c and 5f) also peak in the afternoon, a little earlier than CO_2^+ and the organic mass. This afternoon peak in number concentration occurs when EC reaches its lowest concentrations on both HG and LG days. Also, there is no peak in the multiday-average number concentration during the early morning rush hour on HG or LG days suggesting that primary aerosol emissions do not provide the source of aerosol particles on most days. In fact, a peak in number concentration during rush hour, around 07:00 in the morning, could only be observed on seven days in total. However, on all of those seven days there was an even larger maximum in number concentration during early afternoon. The fact that the peak of the median diurnal cycle for number concentration occurs during afternoon, when EC is at minimum and when the mixed layer is close to fully developed, indicates that new particle formation was likely the most important midday particle number source in Bakersfield during this study and that photochemistry played an important role in the formation.

[36] The number concentration on average increased by over 100% from 10000 cm^{-3} to ~20000 cm^{-3} between 08:00 and 14:00 on HG days, and from 7000 cm^{-3} to ~15000 cm^{-3} between 09:00 and 14:00 on LG days. Figures 5c and 5f also include the condensation sink, which could be expected to be lower on HG days than on LG days at the start time of particle formation and growth. There is a small dip in the median condensation sink between 08:00 and 11:00 on HG days. However, the 25th-percentile of the *CS* in Figure 5f shows that there were low *CS* values in the morning also on several LG days, and as will be discussed in section 3.5, no correlation between low condensation sink in the morning and high particle mass (or number) concentration in the afternoon was found.

[37] New particle formation appears to dominate over primary aerosol emission in producing seed particles for the frequently observed ultrafine growth events in this study. The nucleation mode appeared on most days between 08:00 and 10:00 whereas EC peaked already between 06:00 and 08:00 in the morning. While the EC concentration on most days decreased between 08:00 and 10:00, the particle number concentration rapidly increased in the same time interval. Even on those six days without any clear growth events, the particle number concentration peaked around noon or in early afternoon. These peaks indicate that nucleation events may have occurred also on those days, but that these events

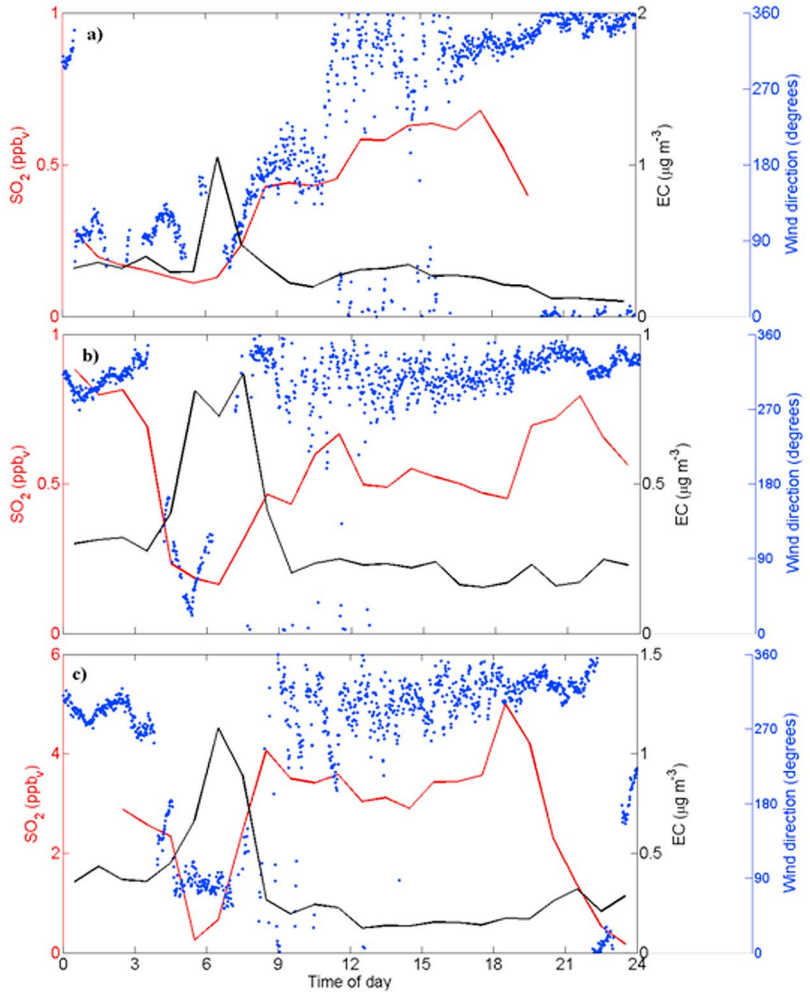

Figure 6. SO_2, EC and wind directions on (a) 25 May, (b) 1 June and (c) 11 June.

must have been local rather than occurring over regional scales.

3.4. Sulfuric Acid Versus Organics in Contributing to Condensational Growth

[38] Organics represented 77% and sulfate only 16% of the ultrafine particle mass. To estimate what role sulfate may have played in the observed growth events, H_2SO_4 condensational growth was investigated by using ambient SO_2 and OH concentrations.

[39] Interestingly, SO_2 did not peak during rush hour (around 07:00 in the morning) when EC and $C_4H_9^+$ were at maximum, indicating that traffic in Bakersfield was not a major source of SO_2. Actually SO_2 was often at minimum at this time in the morning. This seems to have been a result of the often changing wind direction at night or in early morning (section 2.1), particularly clear on 25 May, 1 June and 11 June (Figure 6). When the wind was blowing from the east or south at night or in early morning, the SO_2 concentration dropped significantly but increased as the wind direction returned to the northwest in daytime. The early morning peaks in EC, however, seemed to be independent of wind direction since these occurred during most mornings of the campaign regardless of wind direction.

[40] To investigate what role H_2SO_4 played in the observed condensational growth (after new particle formation) a microphysical model was used. The model includes only growth caused by condensation and uses the standard condensation equation [e.g., *Seinfeld and Pandis*, 1998] with the transition regime correction according to *Fuchs and Sutugin* [1971]. The condensational flux of vapor to particles is driven by the difference between the vapor concentration and its saturation concentration over the particle surface. This saturation concentration was set to zero, thereby assuming sulfuric acid to be perfectly non-volatile. The diffusion coefficient for sulfuric acid was assumed to be 0.1 $cm^2\ s^{-1}$ and the mass accommodation coefficient was assumed to be unity. The model was initiated with a lognormal fit to the 08:00–10:00 average particle number size distribution from Figure 3a, based on three modes. A new nucleation mode was added every hour in order to describe the average increase in particle number concentration observed (as in Figure 3a) between 08:00–10:00 and 12:00–14:00. The sulfuric acid concentration was first held constant at a value that could reproduce the growth in Figure 3a. This was obtained with a H_2SO_4 concentration of $1.1 \cdot 10^8$ molec cm^{-3}. To investigate whether that concentration was realistic at the site, the model

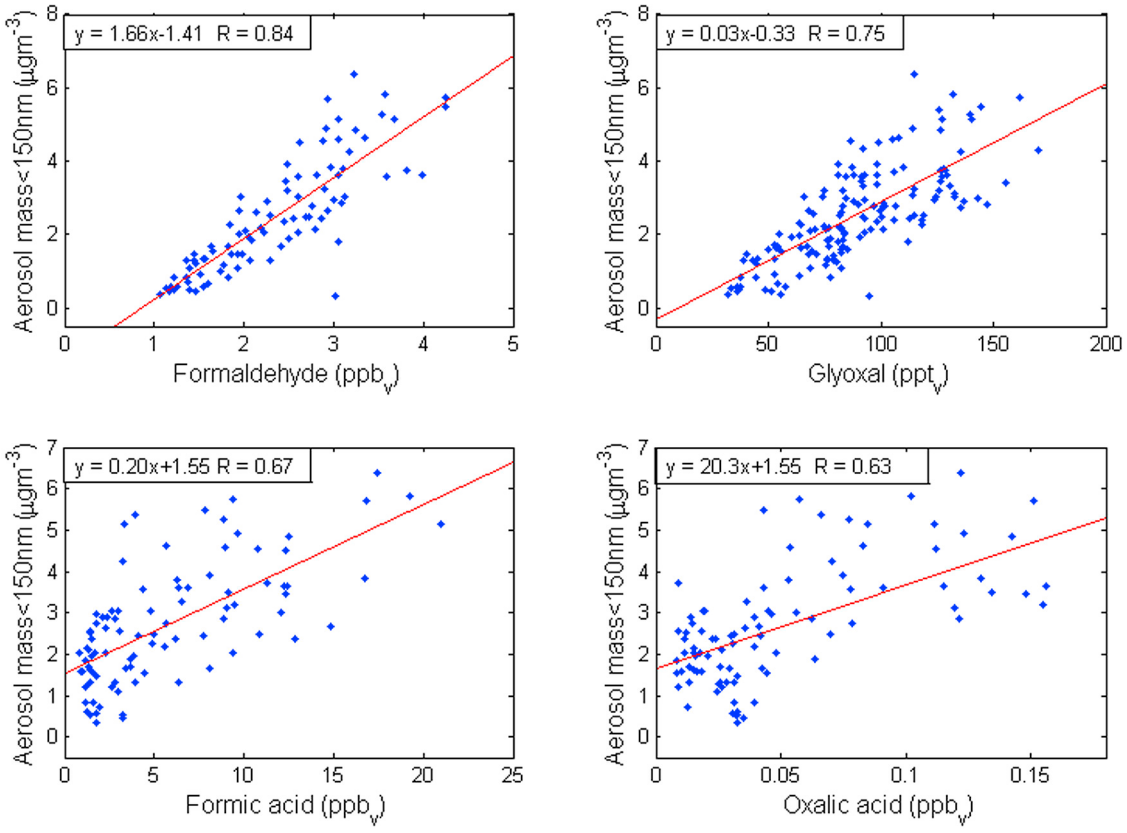

Figure 7. Correlations between aerosol mass of particles smaller than 150 nm and some gas-phase compounds for the time period 09:00 to 14:00.

was run with actual SO_2 and OH concentrations from a median diurnal cycle of these parameters. H_2SO_4 was in the model produced according to the proxy [*Petäjä et al.*, 2009]:

$$H_2SO_4 = \frac{k \cdot |SO_2| \cdot |OH|}{CS} \quad (3)$$

where CS represents the condensation sink and k is defined according to

$$k = 8.6 \cdot 10^{-10} \cdot |OH|^{-0.48} \quad (4)$$

where concentrations have units of molec cm^{-3}, k has the unit cm^3 $molec^{-1}$ s^{-1} and CS has the unit s^{-1}.

[41] Running the model with actual SO_2 and OH concentrations resulted in H_2SO_4 concentrations around $2 \cdot 10^6$ molec cm^{-3}, which is nearly two orders of magnitude lower than what was needed to reproduce the growth. The resulting concentrations of H_2SO_4 from SO_2 and OH in the model could not grow the nucleation mode significantly. Even when the day with highest SO_2 concentrations was used to initialize the SO_2 concentration (with peak at ~5 ppb) the resulting growth during six hours was lower than 5 nm in the model, which is smaller than the ~40 nm observed growth between the 08:00–10:00 and 14:00–16:00 average size distributions in Figure 3a. Thus, SO_2 concentrations were much too low in Bakersfield to explain the observed growth rates in the absence of organics. However, even though organics dominated the ultrafine mass, sulfate still seems to have made a significant contribution on some days, particularly on 4 June (Figure 4).

3.5. Parameters Affecting Condensational Growth and Particle Number Concentration

[42] Condensational growth of ultrafine particles can be expected to be more efficient when background aerosol concentrations of Aitken and accumulation mode particles are low, since these particles represent a surface for vapors to condense on, thereby reducing the amount of vapor that condenses on the growing ultrafine particles. However, in this study no clear dependence on low submicron condensation sink in the morning, and high mass of particles smaller than 150 nm in the afternoon was observed, indicating that condensation sink was less important than other parameters to be discussed. To analyze what parameters and compounds were important for the growth events, correlations between aerosol mass of particles smaller than 150 nm and several other parameters were investigated. One hour averages of the aerosol mass were calculated for the time period 09:00 to 14:00 for all growth events. During this time period the aerosol mass was generally increasing. After 14:00 on several days, the aerosol mass was observed to start decreasing as a result of decreasing number concentration despite continued growth.

[43] The fact that the peak in the AMS ion CO_2^+ and organic mass below 150 nm often reached maximum in the afternoon (Figure 5) indicates that photo-oxidation played an

important role in the secondary aerosol formation associated with the growth events. The correlation coefficient (R) between aerosol mass and OH concentration was 0.51 and the corresponding coefficient between aerosol mass and ozone was 0.33 suggesting that OH played a more important role than ozone in oxidation of VOCs to organic vapors with low enough volatility to contribute to formation of secondary aerosol. The R coefficient between aerosol mass and UV radiation was 0.49. Because OH production depends directly on solar radiation it is logical that the correlation coefficients for OH and UV radiation with aerosol mass have similar values.

[44] No correlation was observed for SO_2 (R = 0.16), consistent with the expectations from the modeling of sulfate condensation (section 3.4). Acetone, which has a variety of primary (biogenic and anthropogenic) and secondary sources around Bakersfield shows some correlation (R = 0.52) with particle mass during growth events suggesting coincident photochemical production of acetone and condensable vapors. The correlation of particle mass during growth events with gas-phase ammonia was similar (R = 0.58). However, the strongest correlations were between aerosol mass and gas-phase formaldehyde (R = 0.84), glyoxal (R = 0.75), formic acid (R = 0.67), and oxalic acid (R = 0.63), indicating that these vapors may have contributed significantly to condensational growth or at least been co-produced by the chemical reactions that produced condensable vapors. Figure 7 shows the dependence of aerosol mass on these vapors with linear fits and associated slopes and intercepts. Formaldehyde was measured between 20 May and 9 June. It is the most abundant aldehyde in the troposphere and can be directly emitted from biomass burning and fossil fuel combustion, or it can be produced by oxidation of both biogenic and anthropogenic hydrocarbons [*Liu et al.*, 2007]. However, there was no indication of any influence from biomass burning during this campaign. Because of its relatively short atmospheric lifetime, typically 2–4 h during the day [*Fried et al.*, 1997; *Wert et al.*, 2003], formaldehyde is a key indicator of recent atmospheric photochemical activity [*Dasgupta et al.*, 2005]. Therefore, the correlation between aerosol mass and formaldehyde during the growth events does not indicate that formaldehyde has been an important contributor to the growth, but probably instead indicates that photochemical oxidation of VOCs was high during the events. Direct emissions of formaldehyde might have played a role, but these emissions could not have been associated with primary particles (such as EC), since EC did not correlate with particle mass in this study.

[45] Glyoxal forms as a first generation oxidation product from numerous VOCs, including aromatic hydrocarbons in polluted air [*Volkamer et al.*, 2006]. Despite its high volatility, there is growing evidence that glyoxal may also contribute to SOA formation [*Liggio et al.*, 2005; *Volkamer et al.*, 2007].

[46] Oxalic acid is the most abundant dicarboxylic acid in the atmosphere and can be emitted from fossil fuel combustion [*Carlton et al.*, 2007] and formed through gas-phase photo-oxidation of VOCs [*Kerminen et al.*, 2000]. Aqueous-phase photo-oxidation of glyoxal is also a potentially important product of oxalic acid [*Carlton et al.*, 2007], but since relative humidity and cloudiness were low during this campaign in Bakersfield, the latter source was probably not important in this study. Due to the presence of two carboxyl groups, dicarboxylic acids have low volatility and are often found in the particle phase [*Chebbi and Carlier*, 1996]. Oxalic acid has been observed to have the highest particle phase concentration of all dicarboxylic acids in several urban studies [e.g., *Kawamura and Ikushima*, 1993; *Sempére and Kawamura*, 1994], and may well have contributed to condensational growth in this study.

[47] In addition to the already mentioned gas-phase compounds, potential correlations between particle mass and 16 alkanes, 6 aromatics, 4 halocarbons, 3 CFCs, alpha-pinene, isoprene, limonene, propene, and carbon disulfide were investigated, but all resulted in correlation coefficients lower than 0.45.

[48] Additional parameters that could be important for new particle formation were also investigated. No clear correlation could be found between ultrafine particle number and relevant parameters such as condensation sink and O_3 concentration between 09:00 and 14:00. However, ultrafine particle number was mildly correlated with UV radiation and OH with R coefficients of 0.51 and 0.43, respectively. SO_2 concentrations in this study were in general relatively low, on most days below 1 ppb_v. This can be compared with SO_2 concentrations in other urban studies with nucleation and growth events, for instance Pittsburgh where concentrations were often 40–120 ppb_v [*Zhang et al.*, 2004], Leipzig with daytime peaks around 8ppb_v [*Birmili and Wiedensohler*, 2000] and Birmingham with concentrations of 1–21 ppb_v. No correlation was observed between particle number and SO_2 concentration (R = 0.14), suggesting that the daytime particle number source did not depend critically on SO_2. This is the third piece of evidence (combined with the sulfate condensation calculations and the composition of the ultrafine particles) that sulfate from SO_2 did not provide most of the particle mass in the high number of particle formation and growth events in this study.

[49] Ammonia concentrations were very high during the campaign, often above 10 ppb_v. A correlation between ultrafine particle number and ammonia was observed with an R-coefficient of 0.45, indicating that ammonia might have played a role in new particle formation in this study. *Kirkby et al.* [2011] found that the dependence of nucleation rates on ammonia saturates at ammonia mixing ratios around 100 ppt_v. The fact that Bakersfield had ammonia concentrations in the ppb-range in this study might explain the relatively low correlation with ammonia.

[50] A higher correlation was observed between ultrafine particle number and formaldehyde (R = 0.62). Relatively high correlations were also observed between ultrafine particle number and oxalic acid (R = 0.59) and formic acid (R = 0.57), whereas the rest of the gas-phase compounds had correlation coefficients lower than 0.4. A high concentration of formaldehyde indicates high VOC oxidation, thereby likely higher concentrations of condensable organic vapors and more efficient condensational growth. More efficient initial growth will reduce particle number sinks like coagulation and Brownian diffusion. Therefore, the correlation between ultrafine particle number and formaldehyde might indicate that the particle number concentration depended more critically on the efficiency of initial

growth than on amounts of nucleating vapors in this study in Bakersfield.

4. Summary and Conclusion

[51] Physical and chemical properties of ultrafine aerosol particles during the CalNex campaign in Bakersfield from 15 May to 29 June were measured. The focus of this study was on the frequently observed growth events at the site. Condensational growth of small ~20 nm particles up to 40–100 nm occurred on 39 of 45 days. A nucleation mode typically appeared around 09:00 in the morning together with a pre-existing Aitken mode centered around 70–80 nm. Throughout the day the nucleation mode was observed to grow at an average growth rate of 7.3 nm hr^{-1}, resulting in a unimodal size distribution in the evening and at night.

[52] Concentrations of EC and a tracer for hydrocarbon-like organic aerosol ($C_4H_9^+$) were in general higher at nighttime and peaked during rush hour in early morning. Throughout the morning and afternoon concentrations decreased as a result of dilution when the mixed layer grew. This is an indication that the impact of primary aerosol emission on local concentrations was at maximum in early morning during rush hour. However, particle number concentration showed a different pattern and peaked in the afternoon when EC was at minimum. Therefore, new particle formation likely provided the largest contribution to the midday increase in particle number concentration in this study.

[53] Microphysical modeling and size-resolved AMS concentrations showed that organic components dominated the particle growth in the ultrafine mode, and that sulfate on most days only provided a minor contribution to nanoparticle growth. Organic components largely dominated the ultrafine aerosol mass with 77%. The organic mass below 150 nm peaked in the afternoon at the same time as the AMS tracer for oxygenated organic aerosol CO_2^+, indicating that most of this organic mass was photochemically produced SOA. Given the complex mixture of anthropogenic and biogenic VOC sources in the Central Valley, there was insufficient information to accurately apportion the sources of the pre-cursor VOCs, but there are likely contributions from both anthropogenic and biogenic sources.

[54] The aerosol mass of particles smaller than 150 nm showed a stronger correlation to OH concentration and UV radiation than to ozone concentration during the growth events. However, the strongest correlations were found between aerosol mass and gas-phase formaldehyde, glyoxal, formic acid and oxalic acid. This is an indication that these compounds may have either contributed to condensational growth or been produced by the same chemical reactions that produced condensable vapors.

[55] **Acknowledgments.** This work was supported by the California Air Resources Board (CARB), under contract 09–328. The statements and conclusions in this paper are those of the researchers (contractor) and not necessarily those of CARB. The mention of commercial products, their source, or their use in connection with material reported herein is not to be construed as actual or implied endorsement of such products. D.R.G. and A.H.G. also acknowledge ARB contract 08–316. We would also like to thank William H. Brune for providing OH measurements. We also thank John Karlik and the Kern County University of California Cooperative Extension staff for hosting the field site.

References

Alam, A., J. P. Shi, and R. M. Harrison (2003), Observations of new particle formation in urban air, *J. Geophys. Res.*, *108*(D3), 4093, doi:10.1029/2001JD001417.

Birmili, W., and A. Wiedensohler (2000), New particle formation in the continental boundary layer: Meteorological and gas phase parameter influence, *Geophys. Res. Lett.*, *27*(20), 3325–3328, doi:10.1029/1999GL011221.

Carlton, A. G., B. J. Turpin, K. E. Altieri, S. Seitzinger, A. Reff, H.-J. Lim, and B. Ervens (2007), Atmospheric oxalic acid and SOA production from glyoxal: Results of aqueous photooxidation experiments, *Atmos. Environ.*, *41*, 7588–7602, doi:10.1016/j.atmosenv.2007.05.035.

Chebbi, A., and P. Carlier (1996), Carboxylic acids in the troposphere, occurrence, sources, and sinks: A review, *Atmos. Environ.*, *30*, 4233–4249, doi:10.1016/1352-2310(96)00102-1.

Chow, J. C., L.-W. A. Chen, J. G. Watson, D. H. Lowenthal, K. A. Magliano, K. Turkiewicz, and D. E. Lehrman (2006), $PM_{2.5}$ chemical composition and spatiotemporal variability during the California Regional PM_{10}/$PM_{2.5}$ Air Quality Study (CRPAQS), *J. Geophys. Res.*, *111*, D10S04, doi:10.1029/2005JD006457.

Collins, D. R., D. R. Cocker, R. C. Flagan, and J. H. Seinfeld (2004), The scanning DMA transfer function, *Aerosol Sci. Technol.*, *38*, 833–850, doi:10.1080/027868290503082.

Dasgupta, P. K., J. Li, G. Zhang, W. T. Luke, W. A. McClenny, J. Stutz, and A. Fried (2005), Summertime ambient formaldehyde in five U.S. metropolitan areas: Nashville, Atlanta, Houston, Philadelphia, and Tampa, *Environ. Sci. Technol.*, *39*, 4767–4783, doi:10.1021/es048327d.

DiGangi, J. P., et al. (2011), First direct measurements of formaldehyde flux via eddy covariance: Implications for missing in-canopy formaldehyde sources, *Atmos. Chem. Phys.*, *11*, 10,565–10,578, doi:10.5194/acp-11-10565-2011.

Dunn, M. J., J. L. Jimenez, D. Baumgardner, T. Castro, P. H. McMurry, and J. N. Smith (2004), Measurements of Mexico City nanoparticle size distributions: Observations of new particle formation and growth, *Geophys. Res. Lett.*, *31*, L10102, doi:10.1029/2004GL019483.

Fried, A., et al. (1997), Photochemistry of formaldehyde during the 1993 Tropospheric OH Photochemistry Experiment, *J. Geophys. Res.*, *102*(D5), 6283–6296, doi:10.1029/96JD03249.

Fuchs, N. A., and A. G. Sutugin (1971), Highly dispersed aerosols, in *Topics in Current Aerosol Research, Part II*, edited by J. M. Hidy and J. R. Brock, pp. 47–60, Pergamon, New York.

Hallquist, M., et al. (2009), The formation, properties and impacts of secondary organic aerosol: Current and emerging issues, *Atmos. Chem. Phys.*, *9*, 5155–5236, doi:10.5194/acp-9-5155-2009.

Harrison, R. M., and A. M. Jones (2005), Multisite study of particle number concentrations in urban air, *Environ. Sci. Technol.*, *39*, 6063–6070, doi:10.1021/es040541e.

Harrison, R. M., C. Giorio, D. C. S. Beddows, and M. Dall'Osto (2010), Size distributions of airborne particles controls outcome of epidemiological studies, *Sci. Total Environ.*, *409*, 289–293, doi:10.1016/j.scitotenv.2010.09.043.

Huisman, A. J., J. R. Hottle, K. L. Coens, J. P. DiGangi, M. M. Galloway, A. Kammrath, and F. N. Keutsch (2008), Laser-induced phosphorescence for the in situ detection of glyoxal at part per trillion mixing ratios, *Anal. Chem.*, *80*, 5884–5891, doi:10.1021/ac800407b.

Kalafut-Pettibone, A. J., J. Wang, W. E. Eichinger, A. Clarke, S. A. Vay, D. R. Blake, and C. O. Stanier (2011), Size-resolved aerosol emission factors and new particle formation/growth activity occurring in Mexico City during the MILAGRO 2006 Campaign, *Atmos. Chem. Phys.*, *11*, 8861–8881, doi:10.5194/acp-11-8861-2011.

Kawamura, K., and K. Ikushima (1993), Seasonal changes in the distribution of dicarboxylic acids in the urban atmosphere, *Environ. Sci. Technol.*, *27*, 2227–2235, doi:10.1021/es00047a033.

Kerminen, V.-M., C. Ojanen, T. Pakkanen, R. Hillamo, M. Aurela, and J. Meriläinen (2000), Low-molecular-weight dicarboxylic acids in an urban and rural atmosphere, *J. Aerosol Sci.*, *31*, 349–362, doi:10.1016/S0021-8502(99)00063-4.

Ketzel, M., P. Wåhlin, A. Kristensson, E. Swietlicki, R. Berkowicz, O. J. Nielsen, and F. Palmgren (2004), Particle size distribution and particle mass measurements at urban, near-city and rural level in the Copenhagen area and Southern Sweden, *Atmos. Chem. Phys.*, *4*, 281–292, doi:10.5194/acp-4-281-2004.

Kirkby, J., et al. (2011), Role of sulfuric acid, ammonia and galactic cosmic rays in atmospheric aerosol nucleation, *Nature*, *476*, 429–433, doi:10.1038/nature10343.

Kittelson, D. B., W. F. Watts, and J. P. Johnson (2006), On-road and laboratory evaluation of combustion aerosols–Part 1: Summary of diesel engine results, *J. Aerosol Sci.*, *37*, 913–930, doi:10.1016/j.jaerosci.2005.08.005.

Kostenidou, E., R. K. Pathak, and S. N. Pandis (2007), An algorithm for the calculation of secondary organic aerosol density combining AMS and SMPS data, *Aerosol Sci. Technol.*, *41*, 1002–1010, doi:10.1080/02786820701666270.

Kulmala, M., M. Dal Maso, J. M. Mäkelä, L. Pirjola, M. Väkevä, P. Aalto, P. Miikkulainen, K. Hämeri, and C. D. O'Dowd (2001), On the formation, growth and composition of nucleation mode particles, *Tellus, Ser. B*, *53*, 479–490.

Kulmala, M., H. Vehkamäki, T. Petäjä, M. Dal Maso, A. Lauri, V.-M. Kerminen, W. Birmili, and P. H. McMurry (2004), Formation and growth of ultrafine atmospheric particles: A review of observations, *J. Aerosol Sci.*, *35*, 143–176, doi:10.1016/j.jaerosci.2003.10.003.

Liggio, J., S.-M. Li, and R. McLaren (2005), Reactive uptake of glyoxal by particulate matter, *J. Geophys. Res.*, *110*, D10304, doi:10.1029/2004JD005113.

Liu, L., et al. (2007), A photochemical modeling study of ozone and formaldehyde generation and budget in the Po basin, *J. Geophys. Res.*, *112*, D22303, doi:10.1029/2006JD008172.

Moore, G. E., C. Daly, M.-K. Liu, and S.-J. Huang (1987), Modeling of mountain-valley wind fields in the southern San Joaquin Valley, California, *J. Clim. Appl. Meteorol.*, *26*, 1230–1242, doi:10.1175/1520-0450(1987)026<1230:MOMVWF>2.0.CO;2.

Oberdörster, G., R. Gelein, J. Ferin, and B. Weiss (1995), Association of particulate air pollution and acute mortality: Involvement of ultrafine particles, *Inhal. Toxicol.*, *7*(1), 111–124, doi:10.3109/08958379509014275.

Petäjä, T., R. L. Mauldin III, E. Kosciuch, J. McGrath, T. Nieminen, P. Paasonen, M. Boy, A. Adamov, T. Kotiaho, and M. Kulmala (2009), Sulfuric acid and OH concentrations in a boreal forest site, *Atmos. Chem. Phys.*, *9*, 7435–7448, doi:10.5194/acp-9-7435-2009.

Peters, A., E. Wichmann, T. Tuch, J. Heinrich, and J. Heyder (1997), Respiratory effects are associated with the number of ultrafine particles, *Am. J. Respir. Crit. Care Med.*, *155*, 1376–1383.

Pope, C. A., and D. W. Dockery (2006), Health effects of fine particulate air pollution: Lines that connect, *J. Air Waste Manage. Assoc.*, *56*, 709–742.

Riipinen, I., et al. (2011), Organic condensation: A vital link connecting aerosol formation to cloud condensation nuclei (CCN) concentrations, *Atmos. Chem. Phys.*, *11*, 3865–3878, doi:10.5194/acp-11-3865-2011.

Rosenfeld, D. (2006), Aerosols, clouds and climate, *Science*, *312*, 1323–1324, doi:10.1126/science.1128972.

Russell, L. M., R. Bahadur, L. N. Hawkins, J. Allan, D. Baumgardner, P. K. Quinn, and T. S. Bates (2009), Organic aerosol characterization by complementary measurements of chemical bonds and molecular fragments, *Atmos. Environ.*, *43*, 6100–6105, doi:10.1016/j.atmosenv.2009.09.036.

Salma, I., T. Borsós, T. Weidinger, P. Aalto, T. Hussein, M. Dal Maso, and M. Kulmala (2011), Production, growth and properties of ultrafine atmospheric aerosol particles in an urban environment, *Atmos. Chem. Phys.*, *11*, 1339–1353, doi:10.5194/acp-11-1339-2011.

Seinfeld, J. H., and S. N. Pandis (1998), *Atmospheric Chemistry and Physics: From Air Pollution to Climate Change*, John Wiley, Hoboken, N. J.

Sempére, R., and K. Kawamura (1994), Comparative distributions of dicarboxylic acids and related polar compounds in snow, rain and aerosols from urban atmosphere, *Atmos. Environ.*, *28*, 449–459, doi:10.1016/1352-2310(94)90123-6.

Shi, J. P., A. A. Khan, and R. M. Harrison (1999), Measurements of ultrafine particle concentration and size distribution in the urban atmosphere, *Sci. Total Environ.*, *235*, 51–64, doi:10.1016/S0048-9697(99)00189-8.

Smith, J. N., M. J. Dunn, T. M. VanReken, K. Iida, M. R. Stolzenburg, P. H. McMurry, and L. G. Huey (2008), Chemical composition of atmospheric nanoparticles formed from nucleation in Tecamac, Mexico: Evidence for an important role for organic species in nanoparticle growth, *Geophys. Res. Lett.*, *35*, L04808, doi:10.1029/2007GL032523.

Stanier, C. O., A. Y. Khlystov, and S. N. Pandis (2004a), Ambient aerosol size distributions and number concentrations measured during the Pittsburgh Air Quality Study (PAQS), *Atmos. Environ.*, *38*, 3275–3284, doi:10.1016/j.atmosenv.2004.03.020.

Stanier, C. O., A. Y. Khlystov, and S. N. Pandis (2004b), Nucleation events during the Pittsburgh Air Quality Study: Description and relation to key meteorological, gas phase, and aerosol parameters, *Aerosol Sci. Technol.*, *38*, 253–264, doi:10.1080/02786820390229570.

Stolzenburg, M. R., P. H. McMurry, H. Sakurai, J. N. Smith, R. L. Mauldin, and F. L. Eisele (2005), Growth rates of freshly nucleated atmospheric particles in Atlanta, *J. Geophys. Res.*, *110*, D22S05, doi:10.1029/2005JD005935.

Volkamer, R., J. L. Jimenez, F. San Martini, K. Dzepina, Q. Zhang, D. Salcedo, L. T. Molina, D. R. Worsnop, and M. J. Molina (2006), Secondary organic aerosol formation from anthropogenic air pollution: Rapid and higher than expected, *Geophys. Res. Lett.*, *33*, L17811, doi:10.1029/2006GL026899.

Volkamer, R., F. San Martini, L. T. Molina, D. Salcedo, J. L. Jimenez, and M. J. Molina (2007), A missing sink for gas-phase glyoxal in Mexico City: Formation of secondary organic aerosol, *Geophys. Res. Lett.*, *34*, L19807, doi:10.1029/2007GL030752.

Wert, B. P., et al. (2003), Signatures of terminal alkene oxidation in airborne formaldehyde measurements during TexAQS 2000, *J. Geophys. Res.*, *108*(D3), 4104, doi:10.1029/2002JD002502.

Woo, K. S., D. R. Chen, D. Y. H. Pui, and P. H. McMurry (2001), Measurement of Atlanta aerosol size distributions: Observations of ultrafine particle events, *Aerosol Sci. Technol.*, *34*, 75–87.

Wu, Z., M. Hu, S. Liu, B. Wehner, S. Bauer, A. Ma Bling, A. Wiedensohler, T. Petäjä, M. Dal Maso, and M. Kulmala (2007), New particle formation in Beijing, China: Statistical analysis of a 1-year data set, *J. Geophys. Res.*, *112*, D09209, doi:10.1029/2006JD007406.

Zaremba, L. L., and J. J. Carroll (1999), Summer wind flow regimes over the Sacramento Valley, *J. Appl. Meteorol.*, *38*, 1463–1473, doi:10.1175/1520-0450(1999)038<1463:SWFROT>2.0.CO;2.

Zhang, Q., C. O. Stanier, M. R. Canagaratna, J. T. Jayne, D. R. Worsnop, S. N. Pandis, and J. L. Jimenez (2004), Insights into the chemistry of new particle formation and growth events in Pittsburgh based on aerosol mass spectrometry, *Environ. Sci. Technol.*, *38*, 4797–4809, doi:10.1021/es035417u.

Zhang, Q., M. R. Alfarra, D. R. Worsnop, J. D. Allan, H. Coe, M. R. Canagaratna, and J. L. Jimenez (2005), Deconvolution and quantification of hydrocarbon-like and oxygenated organic aerosols based on aerosol mass spectrometry, *Environ. Sci. Technol.*, *39*, 4938–4952, doi:10.1021/es048568l.

Zhong, S., C. D. Whiteman, and X. Bian (2004), Diurnal evolution of three-dimensional wind and temperature structure in California's Central Valley, *J. Appl. Meteorol.*, *43*, 1679–1699, doi:10.1175/JAM2154.1.

L. Ahlm, S. Liu, and L. M. Russell, Scripps Institution of Oceanography, University of California, San Diego, La Jolla, CA 92093-0532, USA. (lmrussel@ucsd.edu)

D. A. Day, Cooperative Institute for Research in the Environmental Sciences, University of Colorado at Boulder, Boulder, CO 80309, USA.

J. P. DiGangi, S. B. Henry, and F. N. Keutsch, Department of Chemistry, University of Wisconsin-Madison, 1101 University Ave., Madison, WI 53706, USA.

D. R. Gentner, Department of Civil and Environmental Engineering, University of California, Berkeley, CA 94720-1712, USA.

A. H. Goldstein and R. Weber, Department of Environmental Science, Policy, and Management, University of California, Berkeley, 151 Hilgard Hall, Berkeley, CA 94720-3110, USA.

M. Z. Markovic, J. G. Murphy, and T. C. VandenBoer, Department of Chemistry, University of Toronto, 80 St. George St., Rm. 248, Toronto, Ont M5S 3H6, Canada.

X. Ren, Air Resources Laboratory, National Oceanic and Atmospheric Administration, 1315 East West Hwy., SSMC#3, Rm. 3316, Silver Spring, MD 20878, USA.

S. Scheller, California Air Resources Board, PO Box 2815, Sacramento, CA 95812, USA.